Nickel-modified poly(aniline-co-pyrrole) as electrocatalyst for electrochemical oxidation of methanol in direct methanol fuel cell application

Asha Raveendran[1] · M. Jeyapriya[2] · Chennan Ramalingan[2] · Gopinath Ramamoorthy[3] · Mijun Chandran[4] ·
D. Kamalakannan[5] · B. Prabu[5] · Masoom Raza Siddiqui[6] · Saikh Mohammad Wabaidur[6] ·
Ragupathy Dhanusuraman[1,7]

Abstract

The construction and assessment of an effective, cost-efficient anode catalyst for methanol oxidation reactions (MOR) are crucial in direct methanol fuel cells (DFMC) applications. This work unveils a quick, simple, yet effective method for synthesizing poly(aniline-co-pyrrole) using the "chemical oxidative polymerization" technique and creates an affordable and stable anode catalyst for DMFC applications. The chemical oxidative polymerization approach was employed to copolymerize aniline and pyrrole with incorporation of nickel, and the electrocatalyst showcased remarkable activity towards methanol oxidation reaction (MOR). Physiochemical characterizations such as scanning electron microscopy, FT-infrared spectroscopy, Raman spectroscopy, and thermogravimetric analysis were performed to validate the incorporation of transition metal nickel into the copolymerized conducting polymers (aniline-co-pyrrole), abbreviated as PANiPPy. Electrochemical techniques like cyclic voltammetry, chronoamperometry, and electrochemical impedance spectroscopy (EIS) were used to investigate the capability of the electrocatalysts to oxidize methanol in alkaline conditions. The electrode material NiPANiPPy displayed a higher oxidation current density 280.60 mA/cm^2 from the cyclic voltammogram of the electrocatalysts in 1 M KOH + 1 M methanol compared to the other synthesised electrocatalysts since nickel provides a low onset potential while the copolymers PANiPPy provide good conductivity and mechanical stability. Moreover, NiPANiPPy exhibits the lowest current rate loss and a substantially higher current density among them after 3600 s with the highest current density of 100 mAcm^{-2}. NiPANiPPy was also observed to have the lowest solution resistance with 0.8 Ω compared to other electrocatalysts in EIS spectra. Thus, the synthesized electrocatalysts has potential applications as an enhanced anode electrode for DMFC.

Keywords Polyaniline · Pyrrole · Nickel · Methanol oxidation reaction · Nickel foam · DMFC

✉ Ragupathy Dhanusuraman
ragu@pondiuni.ac.in; ragu.nitpy@gmail.com

[1] Nano Electrochemistry Lab (NEL), Department of Chemistry, National Institute of Technology Puducherry, Karaikal 609609, India

[2] Department of Chemistry, School of Advanced Sciences, Kalasalingam Academy of Research and Education, Krishnankoil, Tamil Nadu 626 126, India

[3] Department of Chemistry, Annamalai University, Annamalai Nagar, Tamil Nadu 608 002, India

[4] Department of Chemistry, Central University of Tamil Nadu, Thiruvarur 610005, India

[5] Department of Mechanical Engineering, Puducherry Technological University, Puducherry 605014, India

[6] Chemistry Department, College of Science, King Saud University, Riyadh 11451, Saudi Arabia

[7] Nano Electrochemistry Laboratory (NEL), Central Instrumentation Facility (CIF), School of Physical, Chemical and Applied Sciences, Pondicherry University, Puducherry 605014, India

Introduction

Direct methanol fuel cell (DMFC) is now thought to be one of the most effective substitute energy supply technologies [1–4] owing to its superior energy efficiency, unpretentious construction, less carbon dioxide production, and ease of use and is upcoming alternative along with other energy conversion devices like water splitting [5–8] as well as energy storage devices like supercapacitor [9–14] and batteries [15–17]. The usage of low-cost liquid fuel that is simple to handle, store, and replenish like methanol, which has an energy density comparable to that of petrol, makes DMFC interesting [18, 19]. The activity of DMFCs is greatly influenced by their electrocatalytic activity of both anodic and cathodic region of the fuel cell which includes properties like good proton conductivity and low permeability to reactants [20, 21]. The anodic reaction of DMFC is often considered a sluggish chemical reaction that requires active catalytic sites for both the oxidation of the methanol and the absorbate intermediates thus making commercialisation of DMFC challenging. Therefore, at least three problems must be solved before DMFC can be utilized commercially: (i) currently expensive electrocatalysts like platinum (Pt) or palladium (Pd) alloy are opted faster oxidation of methanol [22], (ii) electrocatalyst poisoning, especially from methanol oxidation products, and (iii) poisoning leads to low catalyst electrocatalytic efficiency. Because of their inherent shortcomings—high cost and low robustness as a result of their lowered resistance to carbon monoxide poisoning—pure platinum electrocatalysts will not be able to commercialize DMFCs [23]. The generated hydroxyl species on the platinum surface oxidize the absorbed carbon monoxide (CO) at a higher potential, significantly slowing down the methanol oxidation reaction process and thus researchers are on the lookout for effective yet inexpensive replacements of anode catalysts for methanol fuel cells [24].

Many transition metals are investigated because of their superior electrochemical activity and inexpensive cost and among them nickel has several uses in electrochemical systems [25]. Nickel and nickel-based heterostructures are regarded as a viable contender among the non-noble group because they are due to its abundance, affordability, and strong electrocatalytic activity and increase the pace at which CO oxidizes via the oxides' surface redox activity [26, 27]. Both inexpensive and oxyphilic, nickel is a useful element. By increasing the adsorbed hydroxyl ions on the electrocatalyst and by supplying adsorbed hydroxyl at a lower potential, nickel can improve methanol oxidation reaction activity by enabling the oxidative desorption of intermediate [28]. However, the metal nanostructures tend to agglomerate during the electrochemical tests, thus reducing the cyclic life and hence a support of these nanostructures that would not just prevent the agglomeration but would enhance the methanol oxidation reaction is often sought after.

Conjugated conductive polymers, commonly referred to as organic polymeric conductors or conductive polymers, are polymeric materials that are intrinsically conductive in the absence of need for conductive fillers [29, 30]. Because of its excellent electrical conductivity, chemical and environmental stability, low cost, and relatively easy synthesis, one of the most researched conducting polymers is polyaniline. Furthermore, PANi was reported to be an effective conducting matrix for enhancing the dispersion of platinum nanostructures, which in turn boosts the stability and electrocatalytic activity. Both chemical and electrochemical oxidative polymerization can be used to synthesis the polymer with ease [31]. Another well-known conducting polymer is polypyrrole (PPy), which is easy to synthesize due to its chemical and mechanical durability. PPy, which has a higher accessible surface area and outstanding stability, has been employed to boost the carbon support's activity and metal dispersion [32]. Since PPy contains a large number of nitrogen heterocycles, its high conductivity, electrochemical stability, and protons-electron conductivity make it potentially useful in fuel cells. Polypyrrole can be produced by a variety of methods, including oxidative chemical, photonic, electrochemical, and catalytic polymerization of pyrrole [33, 34]. These conducting polymers often behave as support for metal nanostructures for various electrochemical applications.

In light of the numerous instances in which nickel has been used as a modified electrocatalyst for the electrooxidation of methanol in potassium hydroxide medium, nickel has become one of the methanol oxidation reaction's most intriguing and affordable catalysts [35]. The authors of this work presents the inclusion of nickel onto copolymerized PANi and PPy, wherein the incorporated nickel raised the current density along with copolymer of aniline and pyrrole, improving the electro oxidation of methanol, demonstrating NiPANiPPy's suitability as an anode electrocatalyst for the direct methanol fuel cell (DMFC) in methanol oxidation reaction.

Experimental

Materials and reagents

Aniline (ANI) monomer (99.5% purity, Aldrich), nickel (II) sulfate hexahydrate, pyrrole (SRL 99%), potassium hydroxide, and all additional organic solvents, including methanol and ammonium persulfate (APS), were of analytical grade quality and acquired from SRL. The aqueous solutions were

prepared using Milli-Q water. Nickel foam utilized in the measurement of 1 cm width, 3 cm height, and 1 mm thickness which were cleaned utilizing acetone and 1 M HCl. The entire work utilizes double-distilled H_2O.

Synthesis

Synthesis of polyaniline (PANi)

First, 100 ml of 1 M HCl was mixed with aniline (0.01 mM) and agitated rapidly for 20 min in ice bath (maintain temperature close to 0 °C). Then, 20 mM of ammonium per sulfate (APS) was added drop wise during the course of the following 2 h while being continuously agitated and dispersed in around 50 ml of 1 M HCl solution. For 12 h at room temperature, the entire setup was shaken. A rapid foaming and a series of color shifts from pale yellow to dark green were seen during the chemical oxidative polymerization process. Lastly, PANi formed was rinsed three or four times with 1 M HCl filtered and left to dry at room temperature for 24 h.

Synthesis of polypyrrole

The first step in the preparation process involved adding 0.02 mM of pyrrole to 100 ml of 1 M HCl and vigorously stirring for 20 min in ice bath. Next, 30 mM of ammonium per sulfate (APS) was added to the 1 M HCl solution, and mixed for 2 h. There was a strong foaming and a sequence of color shifts from pale yellow to dark black when the mixture is continuously agitated for 12 h at room temperature. Following three to four rounds of washing with 1 M HCl, the synthesised polypyrrole was left to dry at room temperature for a full day.

Copolymerization of PANiPPy

After adding aniline (0.01 mM), which had been dissolved in 100 ml of 1 M HCl, the mixture was rapidly agitated for 10 min in ice bath. Subsequently, pyrrole (0.02 mM) was added dropwise to1 M HCl solution (100 ml) and stirred continuously for 20 min. Next, 30 mM of ammonium per sulfate (APS) was added dropwise to 1 M HCl solution (50 ml) and stirred continuously for 2 h. For 12 h at room temperature, the complete setup was stirred. A strong foaming and a sequence of colors, including green and black, were seen during the chemical oxidative polymerization process. After synthesis, it was washed three to four times with 1 M HCl and air dried overnight.

Incorporation of nickel in PANiPPy

Aniline (0.01 mM) and pyrrole (0.02 mM), dissolved in 100 ml of 1 M HCl, were added first, and the mixture was vigorously stirred for 10 min in ice bath. After dissolving 30 mm of ammonium per sulfate (APS) in 1 M HCl solution (50 ml), nickel sulfate (0.2 mM) was added dropwise to 1 M HCl solution (100 ml) and stirred continuously for 2 h. The entire setup was stirred continuously for 12 h at room temperature. A strong foaming and a succession of green color were seen throughout the chemical oxidative polymerization process. This is followed by filtering three to four times with 1 M HCl, and left to dry at room temperature for 24 h. The copolymerisation between aniline and polymer leads to the probable formation of aniline–pyrrole heterodiads [36] and nickel ions are most likely to be bound electrostatically with the lone pair of nitrogen atoms of both polyaniline and polypyrrole (Fig. 1).

Characterizations

Material characterization

SEM analysis was performed on the synthesised materials using a JEOL Neoscope JCM-7000. The Shimadzu IR affinity-1S instrument was used for obtaining Fourier transform
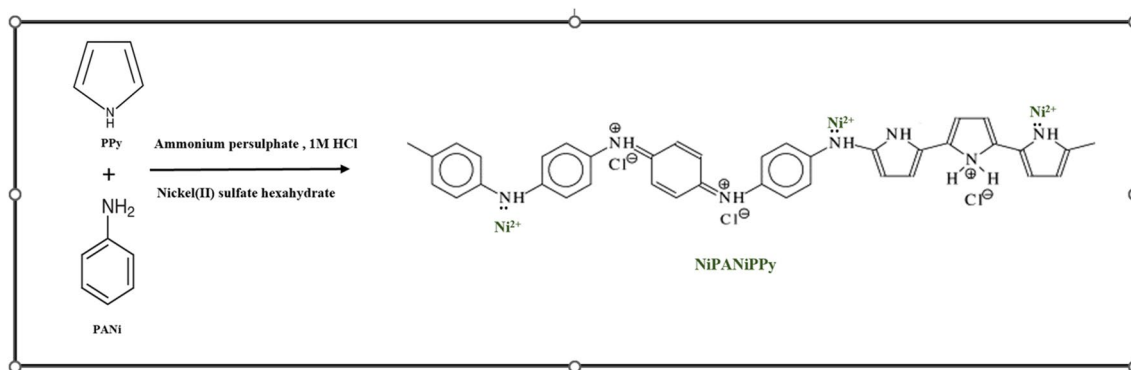

Fig. 1 Schematic diagram of synthesis of NiPANiPPY

infrared (FTIR) spectra in the 4000–400 cm^{-1} range using the KBr pellet method. Raman spectra was derived using Anton Paar Cora 5001 (wavelength 532 nm). Mettler Toledo TGA/DSC 3 + thermal analysis equipment was used to conduct thermogravimetric analysis on the samples.

Electrochemical characterization

The electrochemical performance of the active electrodes was tested using the Metroohm (Multi Auto lab/M204) electrochemical work station. The electrochemical tests were carried out in a three-electrode setup where Pt wire was utilized as counter electrode and Ag/AgCl (3 M KCl) electrode as the reference electrode and nickel foam as working electrode. The electrode material was prepared making a homogeneous slurry of active material (8 mg) with Nafion and ethanol and coated on 1 cm^2 on nickel foam. The working electrode material was then subjected to cyclic voltammetric tests and chronoamperometric tests as well as electrochemical impedance spectroscopy.

Results and discussion

Physio chemical characterization of NiPANiPPy composite

Fourier transform infrared spectroscopy

Figure 2(a) displays the FTIR spectra of the PANi. The band on the quoined ring and benzenoid rings at the C=C

stretching vibrations is identified by the rings that absorb light at 1514 and 1456 cm^{-1} [36]. N–H stretching vibration of PANi's band around 3410 cm^{-1} is main aromatic amine. The identification of the band fall in the 800–860 cm^{-1} region, which is connected to the C-H bond's out-of-plane bending in the 1,4 unsubstituted aromatic rings, has proven crucial in establishing the existence of benzene [37]. The reference band for the carbonyl group is located around 1700 cm^{-1}. The existence of every PANi characteristic peak indicates that aniline has been polymerized successfully. The FTIR spectra of PPy is seen in Fig. 2. The band at 3437 cm^{-1}, 1547 cm^{-1}, and 1396 cm^{-1} is responsible for the existence of the N–H stretching band, the -C=C group stretching, and the C-H stretching vibrations. At 1705 cm^{-1}, the C=O carbonyl group peak was found [38]. The presence of the PPy all-characteristic peaks indicates that the pyrrole polymerization was successful.

The FTIR spectrum of copolymerized PANiPPy is seen in Fig. 2(a). The distinctive band at 1646 cm^{-1} is the consequence of quinoid units undergoing C=N stretching during PANi oxidation. The benzenoid units' C=C stretching deformation mode, which is linked to the polymer's reduced state, is shown by the band at 1500 cm^{-1} [39]. The bands seen at 800–900 cm^{-1}, which are suggestive of para replacement of the aromatic ring, revealed the head-to-tail polymerization process [40]. It is believed that when the emeraldine base is protonated with an acid, quinonoid units experience proton-induced spin-unpairing, which produces benzenoid units. Above 2000 cm^{-1}, protonated emeraldine has a lengthy absorption tail that causes stretching vibration of N–H in the 3100–3500 cm^{-1} range. The C=C stretching
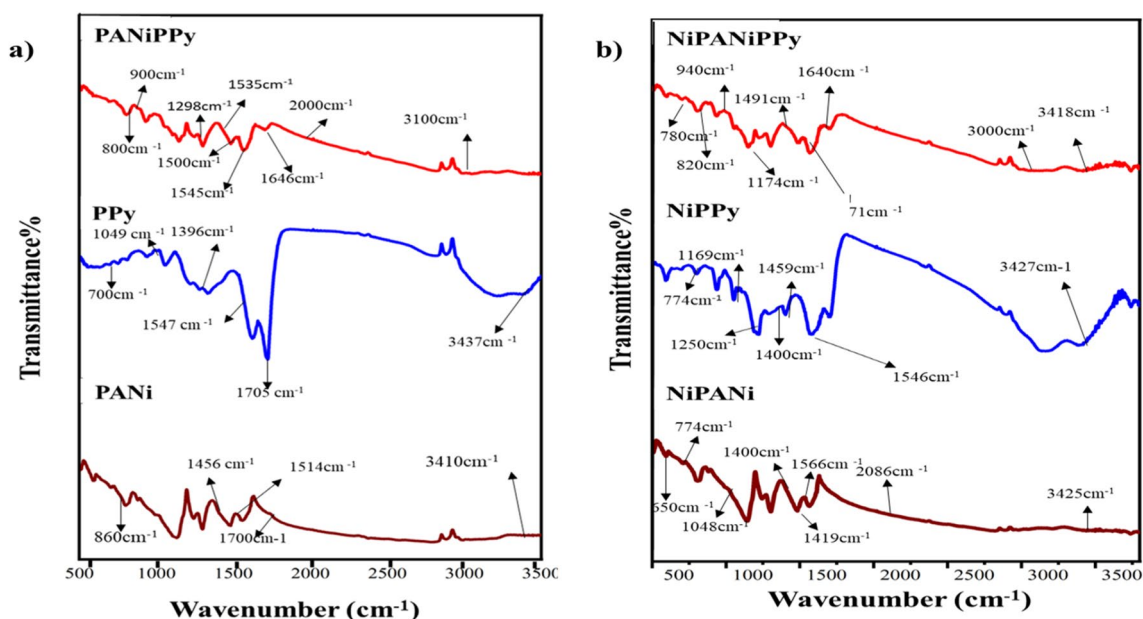

Fig. 2 FTIR spectrum of (a) PANi, PPy, and PANiPPy and (b) NiPANi, NiPPy, and NiPANiPPy

at 1646 cm^{-1} and 1535 cm^{-1}, respectively, is associated with the absorption peaks. The band at 1298 cm^{-1} is caused by the C-N ring stretching [41]. The effective copolymerization of aniline and pyrrole is indicated by the presence of every PANiPPy characteristic peak.

The stretching vibrational peak of NiPANi is responsible for the FTIR spectra displayed in Fig. 2(b), 651 cm^{-1} and 774 cm^{-1}. The C=O groups' vibrational modes are found close to 1400 cm^{-1}. The stretching vibration of the C-N group has been shown to be the absorption band at 2086 cm^{-1}. The quinoid rings of PANi were identified as a vibrational band with a center at 1566 cm^{-1}, and the symmetric stretching vibration of the COO-group was identified as a peak at 1419 cm^{-1}. Polyaniline's N–H stretching vibration exhibited a peak at 3423 cm^{-1}. NiPPy FTIR spectrum's 774 cm^{-1} is a result of Ni's stretching vibrational peak [42]. The absorption peaks of PPy, which were found at 1547 cm^{-1}, 1396 cm^{-1}, and 1169 cm^{-1}, are responsible for the C=C group stretching, stretching vibration of C-H, and C–C stretching vibration of the PPy structure. The bands observed at 1546 and 1459 cm^{-1} are linked with the fundamental vibrations of the pyrrole ring [38]. The broad band between 1400 and 1250 cm^{-1} is ascribed to the in-plane deformation of =C–C modes and the region of the C-N stretching vibrations is seen in 1250 cm^{-1} and 3427 cm^{-1}, corresponding to stretching of N–H the pyrrole ring. In the presence of the NiPANiPPy, 774 cm^{-1} FTIR spectrum is caused by the stretching vibrational peak of nickel. 3418 and 3095 cm^{-1}, respectively, are the N–H and C-H vibrations of the copolymer. At 1630 cm^{-1}, the fundamental vibrations

of the pyrrole ring are visible. It was found that the C-N$^+$ vibrations were represented by the bands at 1174 cm^{-1} [43]. The C-H band's plane bending and vibration are found at 940 cm^{-1}, respectively. Using the C=C stretching of the benzene and quinoid rings as references, the characteristic peaks of PANi were detected at 1490 and 1570 cm^{-1}, respectively [44]. Electron delocalization in PANi backbones resulting from the entire polymerization of aniline is validated by the unique signal suggesting PANi's electron delocalization. The N–H stretching vibrations of PPy chains were discovered to be the source of the absorption peaks at 2999–3405 cm^{-1} [45]. Thus, it was confirmed that PANi and PPy polymeric molecules were present in the generated copolymer.

Raman spectroscopy

The PANi's Raman spectra shows three distinct peaks at 1350 cm^{-1} (belonging to D band), 1584 cm^{-1}, and 1235 cm^{-1} (belonging to G band) in Fig. 3(a) [46]. The peaks were linked with the C=C stretching of the benzenoid ring and in-plane deformation of the C-N band of the quinoid ring, respectively. Figure 3(a) shows that PANi had the fewest possible defects. The Raman spectra of PPy show bands at 940 cm^{-1} and 1059 cm^{-1}, respectively, which are caused by the symmetrical out-of-plane and in-plane bending of the C-H bonds [47].

The pyrrole ring bands that appeared at 1238 cm^{-1} are caused by the N–H in-plane deformation. The strong band associated with C–C stretching at 1586 cm^{-1} represents the

Fig. 3 Raman spectrum of (a) PANi, PPy, and PANiPPy and (b) NiPANi, NiPPy, and NiPANiPPy
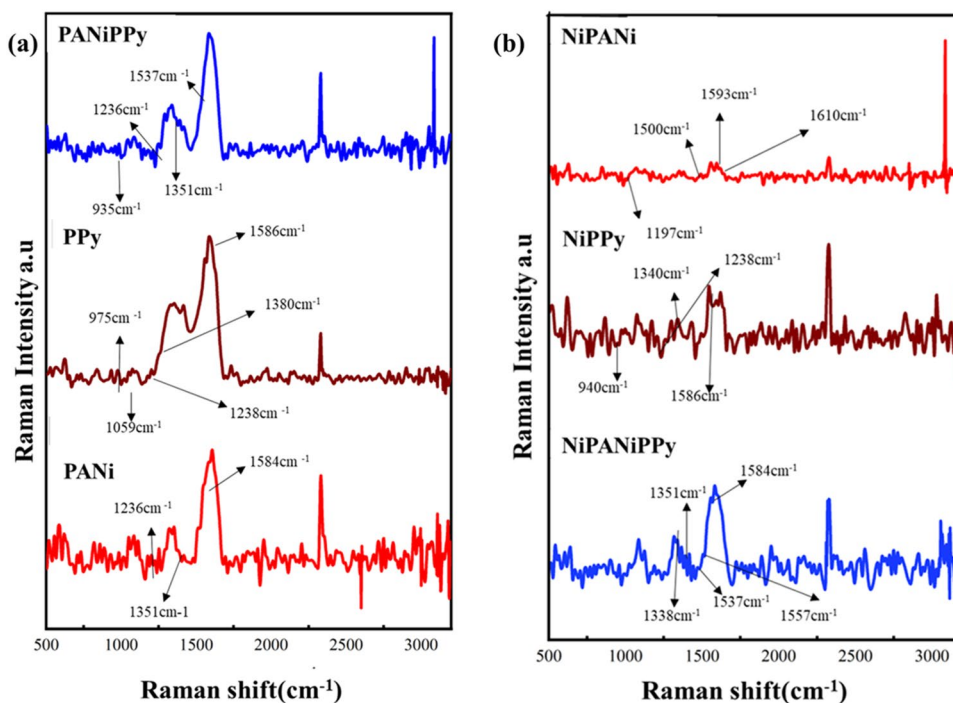
level of doping in PPy chains [48]. These data suggest that PPy is polymerizing. In the case of the copolymer PANiPPy, the wave numbers were different from the PANi and PPy in the following ways: (i) the G band changed from an elevated to a lower area; (ii) the D band moved from a low to a higher position. Symmetric out-of-plane emission can account for the 940 cm^{-1} bands observed in the Ni PPy Raman spectra. Deformation of the N–H plane is the cause of the bands at 1238 cm^{-1}. Around 1340 cm^{-1}, bands began to emerge as a result of the pyrrole's C-N stretching. The strong band, coupled with C–C stretching at 1586 cm^{-1}, shows polypyrrole's level of doping [49]. The peaks at 1351 cm^{-1} (D band) and 1537 cm^{-1} (G band), respectively, in the copolymer's Raman spectra represent the C-N and C–C stretching of the quinoid ring [50]. The $C=N$ stretching vibrations of the unprotonated quinoid ring, the C–C stretching of emeraldine salt, the C-H in-plane bending vibration of the benzenoid ring, observations made on NiPANi's Raman spectra, and 1593 cm^{-1} from in-plane vibration. The Raman spectra of the NiPANiPPy show peaks where PANi contributes to $C=C$, $C=N$, and $C=C$ stretching of the benzenoid ring, as well as three distinct plane deformations of the C-N bond in quinoid ring: 1315 cm^{-1}, 1584 cm^{-1}, and 1236 cm^{-1}. These peaks have the ring stretching mode and the $C=C$ backbone in Fig. 3(b) [51, 52].

Scanning *electron* microscopy and energy-dispersive X-Ray analysis

Scanning electron microscopic images and energy-dispersive X-ray analysis (EDX) are listed in Figs. 4 and 5. The surface morphology and structure of the prepared electrocatalyst in Fig. 4 (a) PANi, (b) PPy, and (c) PANiPPy, and Fig. 5 (a) NiPANi, (b) NiPPy, and (c) NiPANiPPy was achieved using SEM examination. Under low magnification, the NiPANiPPy nanocomposite's morphology is revealed to be heterogeneous, with aggregated particles of the polymers where polypyrrole had granular morphology while polyaniline has an inter-network fiber-like structure accompanied with small spherical nanostructures of nickel. From the SEM images using Image J software, it was derived that the average granule size of polypyrrole is around 500 nm, the average diameters of nanofibers of PANi are around 120 nm, and average diameter of nickel nanoparticles 80 nm. The further confirmation of the nickel nanoparticles' existence was established by the energy-dispersive X-ray (EDX) spectrum, which also confirmed the presence of elements carbon, nitrogen, and nickel in polymers and copolymers of PANi, PPy, PANiPPy, NiPANi, NiPPy, and NiPANiPPy confirmed from Figs. 4 and 5 (d, e, f). Cl ion is also observed which is obtained during the synthesis process. Due to the finer granular morphology of PPy, the surface area for the deposition of nickel nanostructures is comparatively slightly more

than network-like polyaniline and thus %, nickel deposition is higher in NiPPy compared to NiPANi as observed in the EDX spectra of NiPPy and NiPANi.

Thermogravimetric analysis (TGA)

Investigation of pyrolysis processes and thermal stability of polymers is facilitated by thermogravimetric analysis (TGA). Direct alcohol fuel cells often have low operating temperatures and could often go up to 250 °C. Thus, employing TGA analysis gives an insight if the polymers could withstand higher temperatures as well as the changes they undergo with the elevation of temperature. The temperature was heated from 25 to 1000 °C in air at a rate of 10 °C min^{-1} for the TGA measurements of all electrocatalysts in Fig. 6. Heat-induced degradation of the remaining water caused PANi to lose weight initially, while it is estimated that the functional groups in the PANi decomposed between 200 and 300 °C. Heat-induced degradation of the remaining water caused PPy to lose weight initially. Almost 60% weight loss was noted at 1000 °C, while decomposition of PPy was seen at 200 and 600 °C. PANiPPy thermal stability significantly enhanced, which was linked to the copolymerization of PPy with polyaniline. The composite first loses moisture and weights at 254 °C. The polymer film retains its stability up to 1000 °C with 48.8% retention. This leads to the conclusion that the PANiPPy composite is thermally more stable than any of the supported constituents. It is clear that some molecular group realignment has undoubtedly taken place during the composite building process. The TGA analysis of NiPANiPPy is depicted in Fig. 6(f). The first weight losses associated with the NiPANiPPy at around 100 °C may have resulted from the samples, surface-absorbed water molecules evaporating. Following this, NiPANiPPy major weight loss occurs as a result of the NiPANiPPy backbone degrading and was observed to have slightly better stability compared to the polymer due to incorporation of nickel. The copolymerization of polyaniline and polypyrrole helped to enhance the deposition efficiency of Nickel nanostructure, which the thermogravimetric analysis findings verified.

Electrochemical studies

Cyclic voltammograms

Using cyclic voltammograms (CV), chronoamperometry studies (CA), and electrochemical impedance spectroscopy (EIS) of methanol in alkaline medium 1 M KOH, an investigation was conducted on the NiPANiPPy catalyst's electrochemical activity. The electrocatalytic efficiency of PANi, PPy, PANiPPy, NiPANi, NiPPy, and NiPANiPPy was investigated for the electrooxidation of methanol (MOR). Pt wire was utilized as counter electrode and Ag/AgCl(3 M
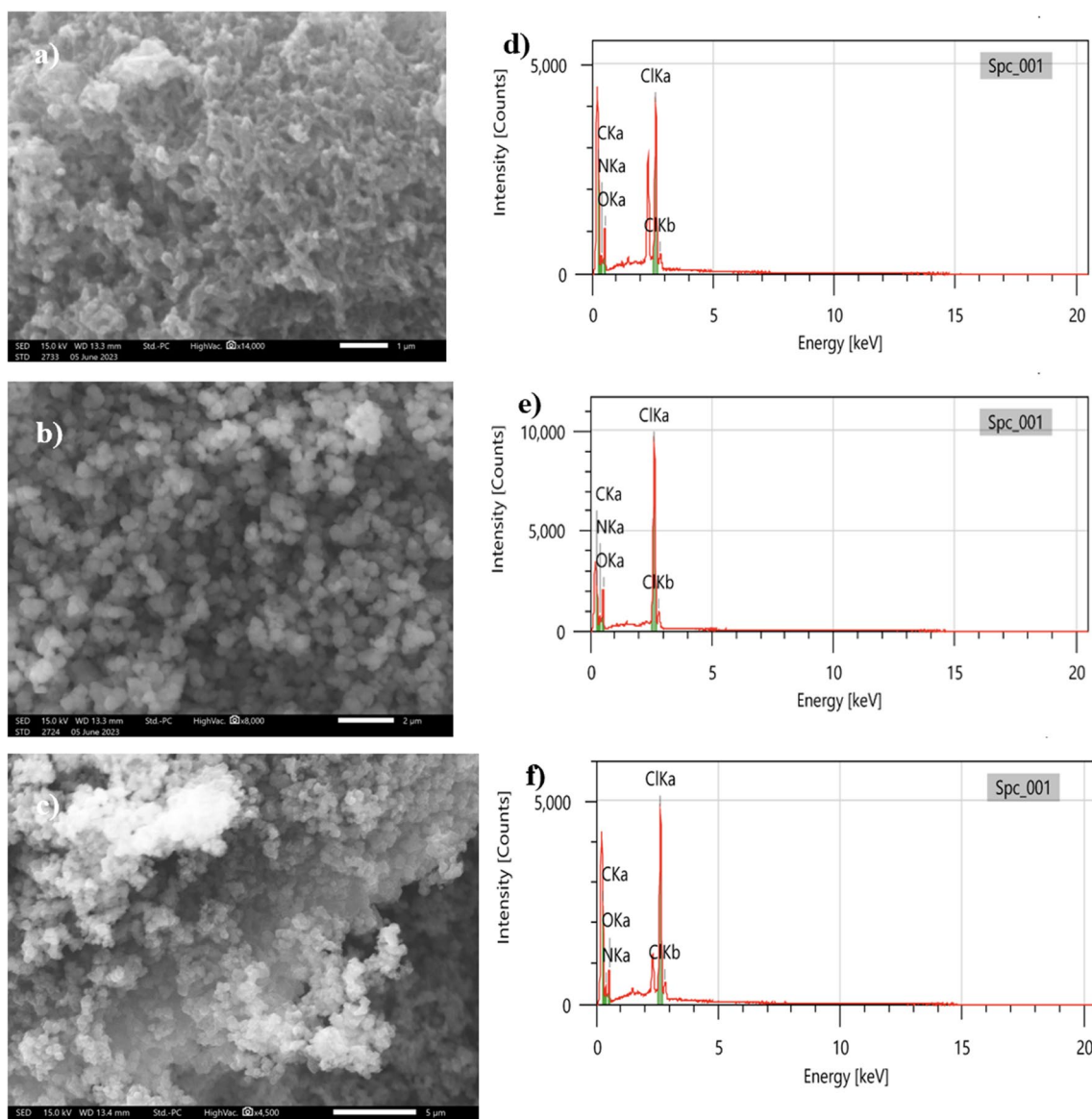
Fig. 4 SEM images and EDX spectra of PANi, PPy, and PANiPPy

KCl)electrode as the reference electrode using Nickel foam as working electrode.

All electrocatalysts had their cyclic voltammograms derived from 1.0 M KOH by scanning the potential window between 0 and 0.7 V at 50 mVs^{-1}, as observed in Fig. 7(a) and (b). Figure 7(c) depicts the cyclic voltammogram of bare nickel foam in presence and absence of methanol in 1 M KOH where there is significant change in shape in cyclic voltammogram in the presence of methanol indicating the methanol oxidation reaction of Ni^{2+} and Ni^{3+} of nickel foam. Figure 8 showcases the cyclic voltammogram of NiPANiPPy and other electrocatalysts with varying scan rates and it was observed that as scan rate increases, current also increases due to the improved diffusion of hydroxyl ions towards the electrode material at higher scan rates. The CV displays an oxidation peak at 400 mV vs. `Ag/AgCl, indicating over-oxidized polypyrrole framework. The reverse scan shows a reduced peak at -250 mV vs. Ag/AgCl indicating reduction of the polypyrrole framework. During the reduction process of polypyrrole, OH- ions may be inserted into the polymer chain, leading to slight increased current density in the reverse scan. During redox reaction, polymer PANi transforms from semi-doped emeraldine to completely doped pernigraniline leading to their anodic and cathodic peaks in the cyclic voltammograms. Anodic and cathodic peaks can be seen in forward and backward scans, respectively: the anodic peak indicates the oxidation of Ni^{3+}, and the
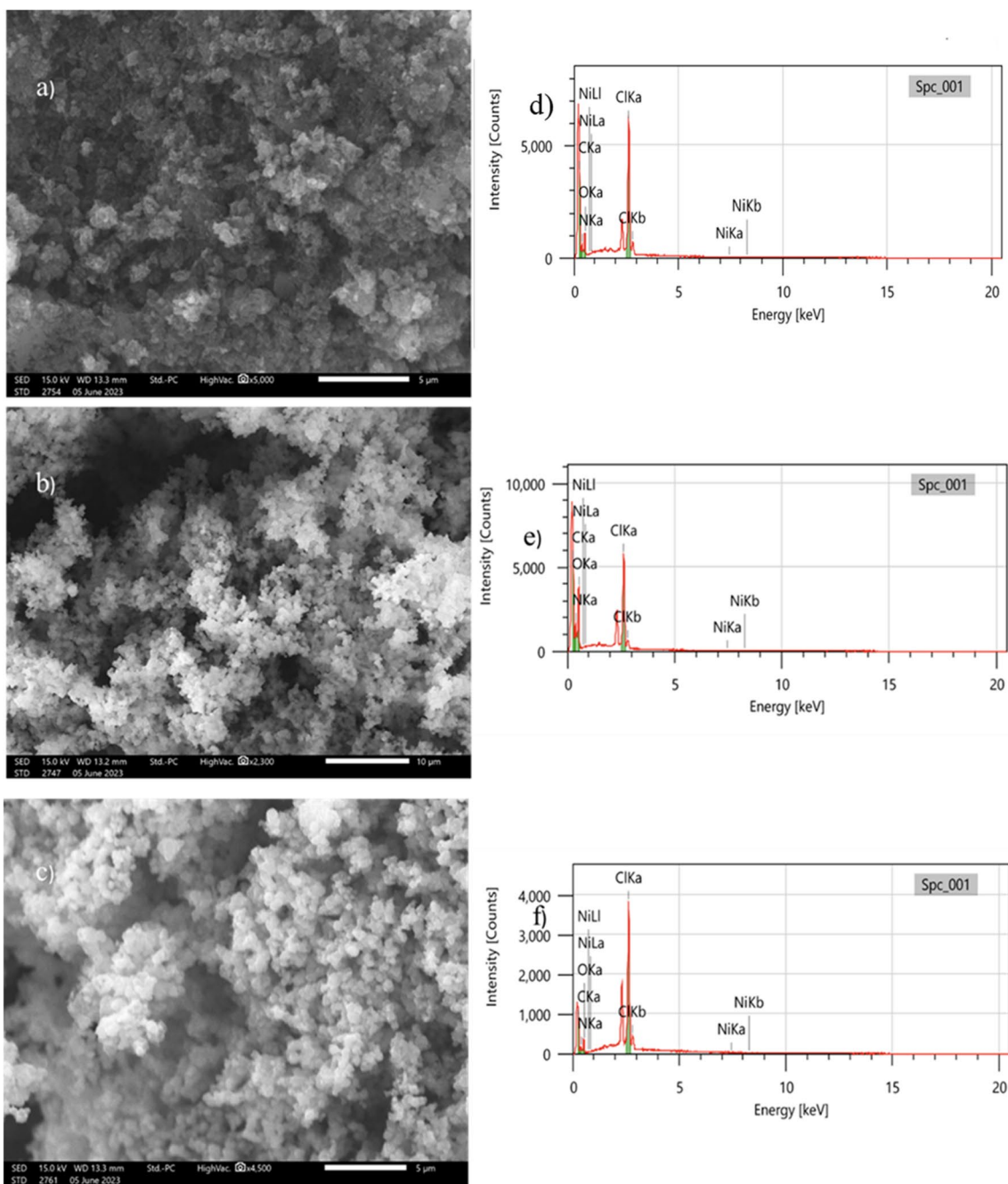
Fig. 5 SEM images and EDX spectra of NiPANi, NiPPy, and NiPANiPPy

cathodic peak indicates the reduction of Ni^{3+} to Ni^{2+} of NiPANiPPy nanocomposite electrodes.The oxidation peak at the potential of 0.45 V has the maximum current density at 65 mAcm^{-2} for the NiPANiPPy and is also accompanied with the highest integral area within the cyclic voltammogram, thereby showing the synergistic effect of the two polymers along with nickel. The possible reaction that occurs during the redox reaction of the final electrode is shown below:

$$[(NiPANiPPy)(OH)_2] + OH^- \leftrightarrow [(NiPANiPPy)OOH] + H_2O + e^-$$
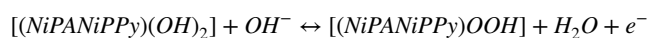
On subjecting PANi, PPy, PANiPPy, NiPANi, NiPPy, and NiPANiPPy to methanol in Fig. 11, cyclic voltammograms of all synthesized electrocatalysts in 1 M KOH to a 1.0 M CH_3OH in 1.0 M KOH to cyclic voltammetry study, they displayed the distinctive oxidation peaks shown in Fig. 9.

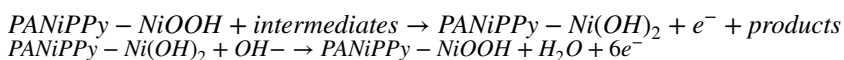The possible reactions in 1 M methanol with 1 M KOH for NiPANiPPy include [53, 54]:
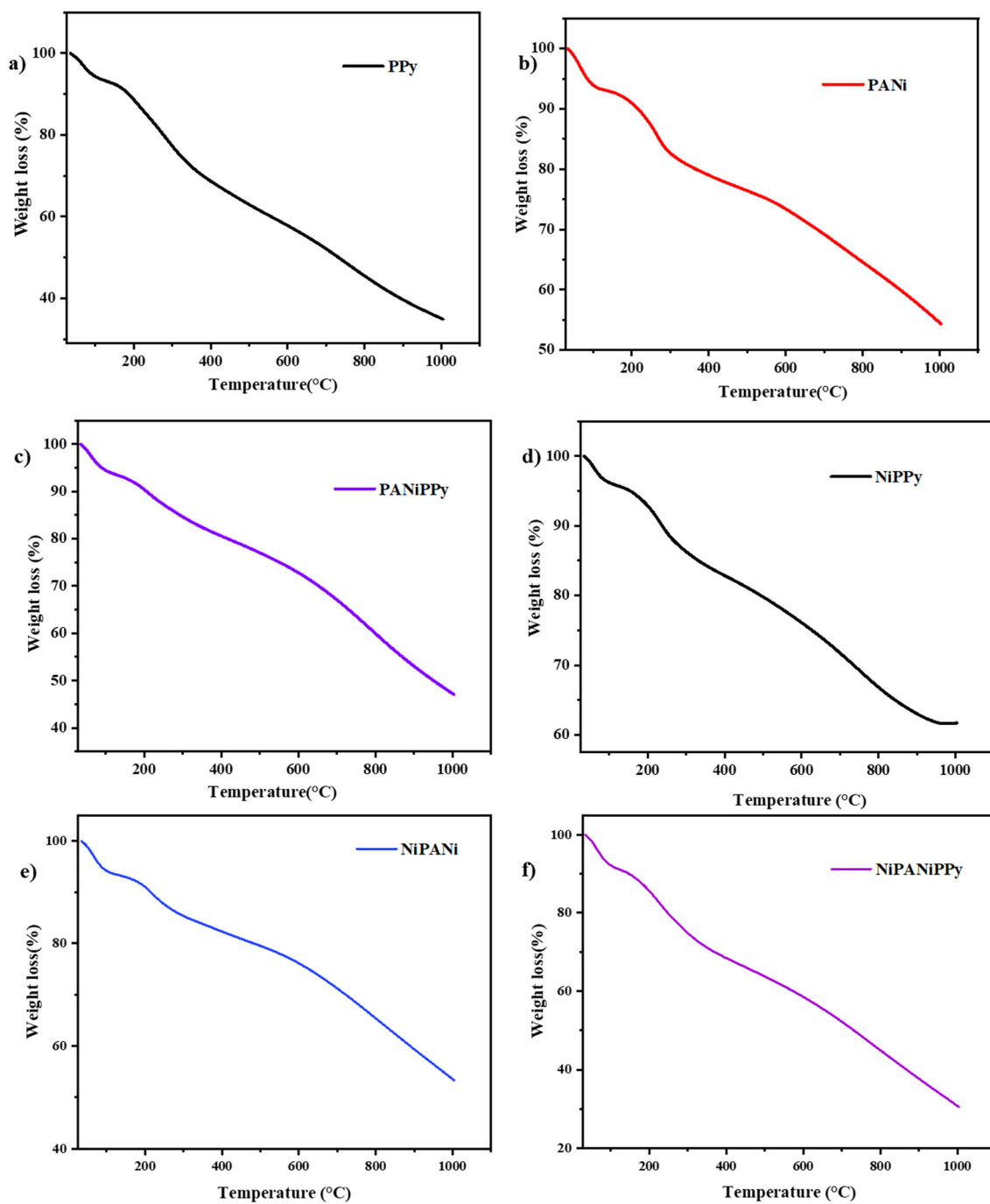
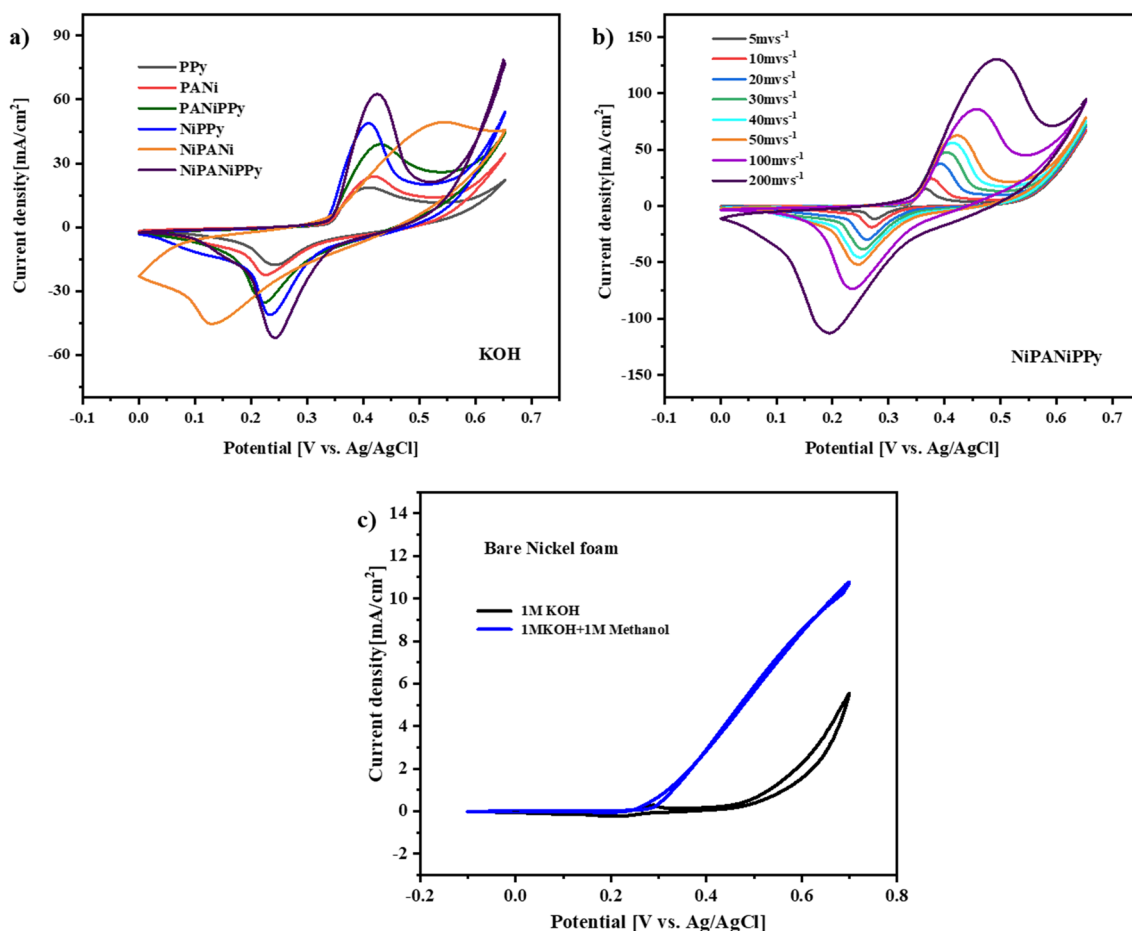**Fig. 6** TGA of (a) PPy, (b) PANi, (c) PANiPPy, (d) NiPANi, (e) NiPPy, and (f) NiPANiPPy

$$PANiPPy - Ni(s) + 2OH^- \rightarrow PANiPPy - Ni(OH)_2 + 2e^- (once immersed)$$

$$PANiPPy - NiOOH + intermediates \rightarrow PANiPPy - Ni(OH)_2 + e^- + products$$
$$PANiPPy - Ni(OH)_2 + OH- \rightarrow PANiPPy - NiOOH + H_2O + 6e^-$$

$$PANiPPy - NiOOH + (CH_3OH)_{ads} \rightarrow PANiPPy - Ni(OH)_2 + e^- + intermediates$$

Fig. 7 (a) Cyclic voltammograms (CV) of all synthesised electrocatalysts in alkaline 1 M KOH. (b) Cyclic voltammogram of NiPANiPPy at varying scan rates. (c) Cyclic voltammogram of bare nickel foam in presence and absence of methanol in 1 M KOH

$$PANiPPy - NiOOH + H_2O + e^- \rightarrow PANiPPy - Ni(OH)_2 + OH^-$$
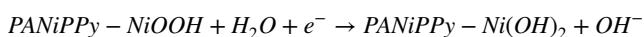
With a better anodic peak at 0.35 V compared to PANi, PPy, PANiPPy, NiPANi, and NiPPy in the forward scan, NiPANiPPy catalyst showed enhanced oxidation peak current density. In the backward scan, there was a decrease in current density of the methanol oxidation and it exhibited the typical methanol oxidation cycle. When methanol is added, the reduction peak vanishes and the oxidation current rises for all electrocatalysts, suggesting that they are more electrocatalytically active than pure KOH solution when it comes to oxidizing methanol. Compared to other electrocatalysts, NiPANiPPy shows the highest oxidation current density of 280 mAcm^{-2} compared to 150 mAcm^{-2}, 143 mAcm^{-2}, 130 mAcm^{-2}, 95 mAcm^{-2}, and 72 mAcm^{-2} of PANiPPy, NiPANi, NiPPy, PANi, and PPy. The onset potential shift that is negative and impacts the adsorption conformations of methanol is primarily caused by the Ni and the copolymerization of PANi and PPy increased the electrical conductivity. This catalytic activity of methanol oxidation was frequently observed for nickel and nickel-altered

electrodes in alkaline conditions. Owing to polyaniline and polypyrrole's copolymerization, electrical charges may move easily. Moreover, in accordance with SEM and EDX data of PPy, their spherical/globular form and network-like structure of PANi that allow for increased surface area are used for the deposition of nickel nanostructures without agglomeration. This allows for improved methanol desorption and adsorption and increased oxidation activity at lower onset potentials [55–57]. The electrooxidation of methanol depends on the adsorption of both intermediates and reactants where the hydroxyl bond is broken resulting in methoxy species line CH_2OH, $CHOH$, and CO. The oxidation of these intermediates is confirmed by the backward oxidation peak of the electrocatalyst while the forward corresponds to the methanol oxidation alone. The peak current density of NiPANiPPy in the presence of methanol was compared with the reported polymer based electrocatalysts in Table 1.

The anodic current density of methanol increased in the presence of the polymeric substrate containing nickel. The copolymer PANiPPy exhibits higher surface roughness and electrical conductivity due to its porous network
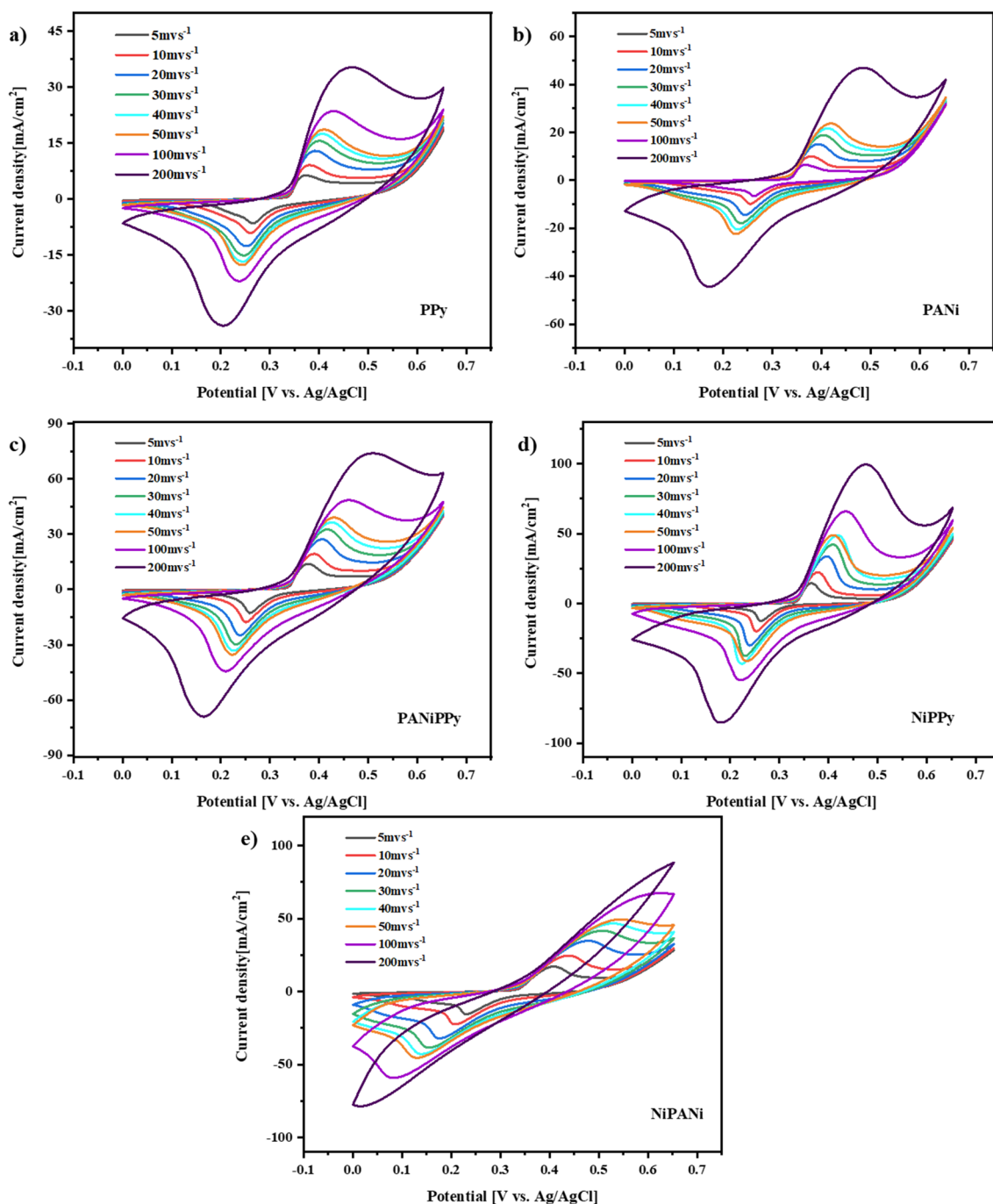
Fig. 8 Cyclic voltammogram of (a) PPy, (b) PANi, (c) PANiPPy, (d) NiPPy, and (e) NiPANi at varying scan rates in 1 M KOH

containing several amine groups. The copolymer of PANi and PPy improved the electron as well as mass transport by preventing the agglomeration of the nickel nanoparticles active sites and protecting the supported nickel nanoparticles from corrosion, thereby increasing the durability of the nickel nanoparticles for methanol oxidation. Moreover, the copolymers PANi and PPy have N atoms in their structure which interacts with the metal nanoparticle and also enhance the electrical conductivity since conducting polymers are electrically conductive materials. In actuality, the metal's electron density is significantly increased due to the nitrogen content, improving the metal's electrical properties. This leads to the synergistic effect between nickel and the copolymer and hence exhibits the highest methanol oxidation peak current density compared to the other electrocatalysts.
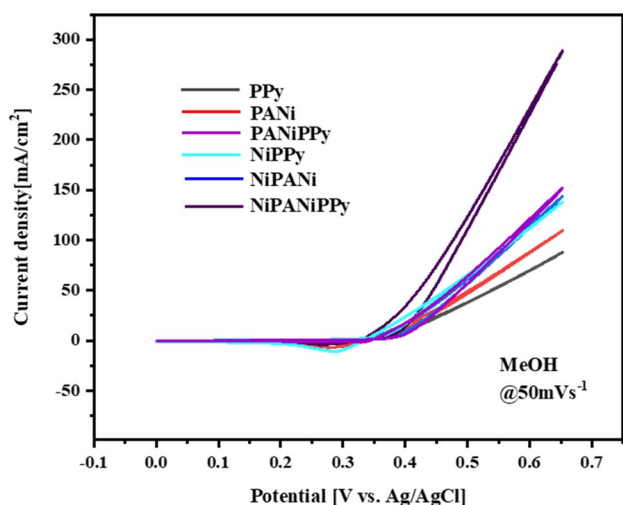
Fig. 9 Cyclic voltammograms of all electrocatalysts in 1 M KOH + 1 M MeOH

Table 1 Comparison of methanol oxidation electroactivity of reported polymer based electrocatalysts with NiPANiPPy

Electrocatalyst	Electrolyte	Anodic peak current density	Ref
Pd/P(Py-ani)	0.5 M KOH	1.79 mA cm^{-2}	[55]
Au/PANi	0.5 M NaOH	3.36 mA cm^{-2}	[58]
Ni/PPy	0.1 M NaOH	3.9 mA cm^{-2}	[59]
Pd/PANi/TiO$_2$	0.5 M KOH	80.12 mA cm^{-2}	[60]
PdPtAu/PPY	1 M KOH	32.35 mA cm^{-2}	[61]
NiPANiPPy	1 M KOH	280 mA cm^{-2}	This work

For a cyclic voltammetry experiment, the impact of scan rate as well as concentration on the peak oxidation current i_p is expressed by the Randles–Sevčík equation. Simple redox processes depend on scan rate in addition to the electroactive component's concentration to confirm their diffusional characteristics.

$$i_p = 0.4463 \, nFAC \left(\frac{nFvD}{RT} \right)^{\frac{1}{2}}$$

i_p: peak current density, A: electrode area, D: diffusion coefficient, v: scan rate n: number of electrons transferred in the redox reaction, F: Faraday constant, C: concentration, T: temperature, R: gas constant.

Peak current increases when methanol concentration and oxidation rate grow, as observed in Fig. 8 for NiPANiPPy which is intended to assess the impact of methanol concentration on methanol oxidation processes of NiPANiPPy at the scan rate of 50 mV/s, where there is also a greater chance of rising carbonaceous intermediates. The increase

in the anodic voltage of Ni(II)/Ni(III) with an increase in concentration of methanol indicates the rate of oxidation of methanol dependency on methanol peak current. This also confirms that NiPANiPPy also follows the Randles–Sevčík equation indicating they are diffusion-controlled process. NiPANiPPy's cyclic voltammograms with varying methanol concentration in 1 M KOH solution are shown in Fig. 10 and of other electrocatalysts are seen in Fig. 11.

NiPANiPPy's cyclic voltammograms with varying scan rates from 5 to 200 mVs^{-1} in a 1 M KOH solution are shown in Fig. 12. It was established that both cathodic and anodic peak intensities increase with increasing scan rate which in accordance with the Randles–Sevčík equation also confirming its diffusion-controlled process. The same was observed for other electrocatalysts too as seen in Fig. 13.

From the linear relationship between current density versus square root of scan rate for methanol oxidation reaction (Fig. 14) which offers insight into the diffusion coefficient obtained by the Randles–Sevcik equation. NiPANiPPy has a diffusion coefficient of 1.11×10^{-5} cm^2 s^{-1} and for methanol oxidation, PANiPPy, NiPANi, NiPPy, PANi, and PPy have values 7.62×10^{-6}, 7.43×10^{-6}, 5.80×10^{-6}, 5.13×10^{-6}, and 1.63×10^{-6} cm^2 s^{-1} respectively, which indicates the employment of a diffusion-controlled process in the methanol oxidation process.

Chronoamperometric studies

Chronoamperometry was used to measure the durability of PANi, PPy, PANiPPy, NiPANi, NiPPy, and NiPANiPPy in a 1 M methanol solution in 1 M KOH up to 3600 s, to analyze the long-term stability is seen in Fig. 15. By maintaining a constant voltage on the working electrode while analyzing current as a function of time, the poison tolerance of all the
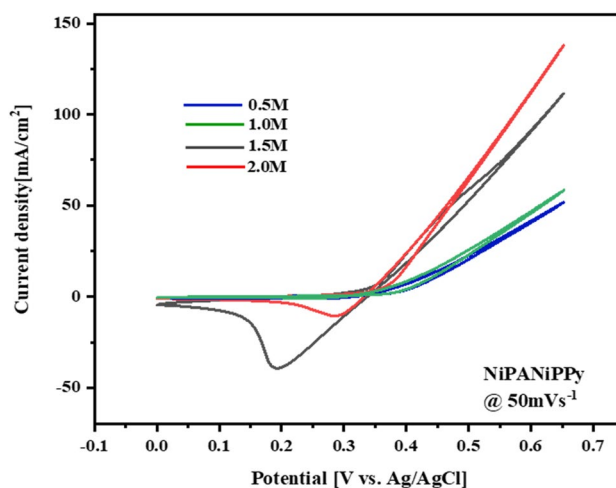

Fig. 10 Cyclic voltammograms (CV) of NiPANiPPy in 1 M KOH at varying methanol concentrations
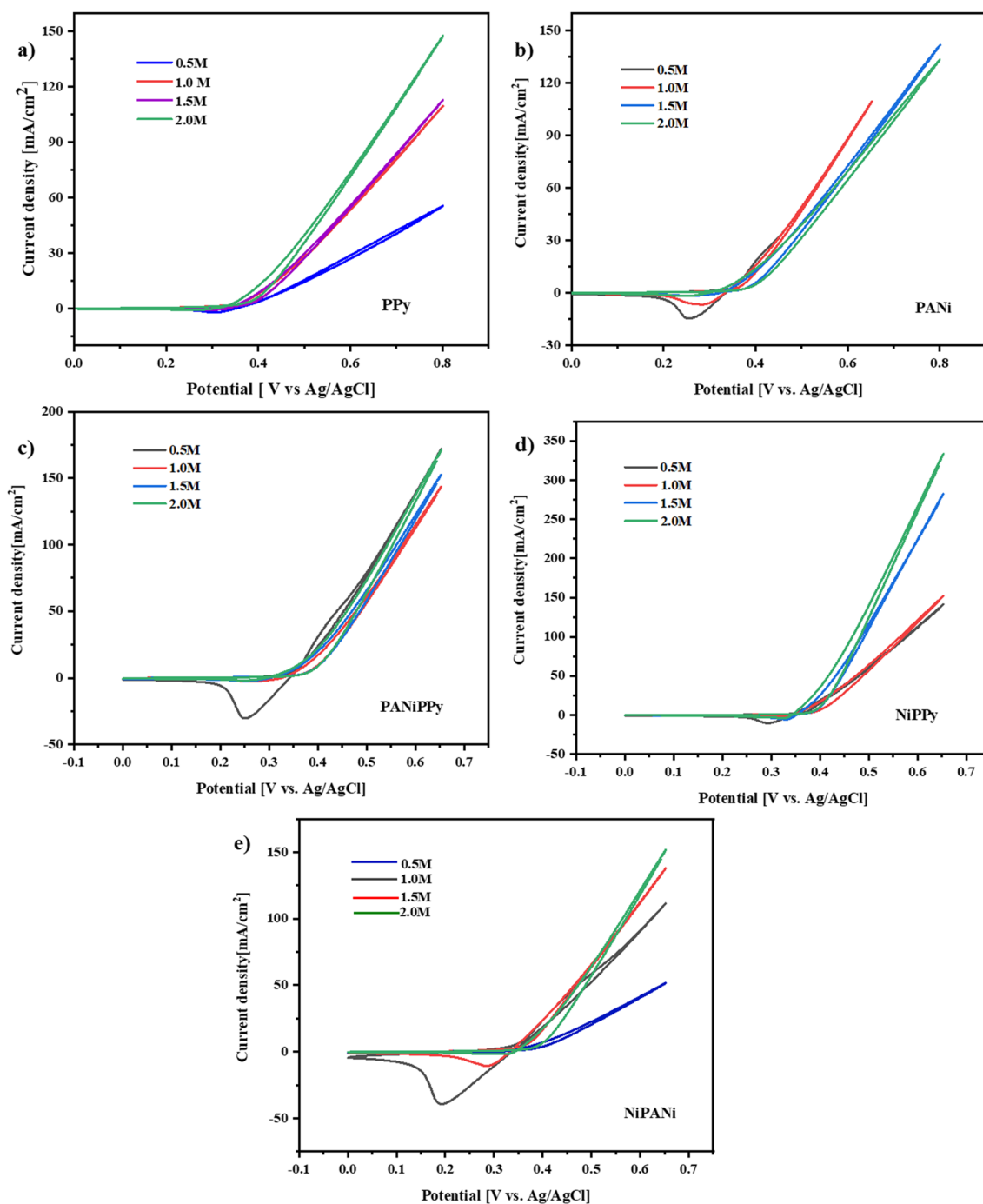
Fig. 11 Cyclic voltammograms of (a) PPy, (b) PANi, (c) PANiPPy, (d) NiPPy, and (e) NiPANi at variable methanol concentration in 1 M KOH

electrocatalysts was evaluated. The current density slightly decreased initially in the chronoamperometry profiles, then it quasi-stabilized, with NiPANiPPy being more stable than all other electrocatalysts.

Catalyst NiPANiPPy exhibits the lowest current rate loss and has a substantially higher current density among them and its seen that, after 3600 s, the highest current density is correlated with 100 mAcm^{-2} for NiPANiPPy. The initial

blockage of active sites was finally maintained by either blocking a specific favored site or establishing equilibrium adsorption/desorption.

EIS impedance spectroscopy

Diffusion and charge transfer behavior in a 0.1 M KOH solution were studied using the EIS technique in the frequency

Fig. 12 Cyclic voltammogram of NiPANiPPy in 1 M KOH + 1 M methanol at varying scan rate

capacitive properties of active materials or interfaces in electrochemical devices. Rp represents the electrical resistance during OH − adsorption on active material on nickel foam, whereas CPE represents the electric double-layer capacitance at the NiPANiPPy interface.

Conclusion

In conclusion, this work utilities chemical oxidative polymerization technique to copolymerize conducting polymers polyaniline and polypyrrole (PANiPPy) with the incorporation of nickel nanostructures and the resultant electrode material, NiPANiPPy, was studied as anode catalyst for direct methanol fuel cell applications. The physiochemical characterizations like FTIR, SEM, Raman spectroscopy, and TGA were carried out to confirm the integration of nickel on the copolymerized PANiPPy conducting polymer. Electrochemical characterizations like cyclic voltammograms, chronoamperometry, and electrochemical impedance spectroscopy methods were used to investigate the electrocatalytic performances of the electrocatalysts PANi, PPy, PANiPPy, NiPANi, NiPPy, and NiPANiPPy. Compared to other electrocatalysts, NiPANiPPy shows the highest oxidation current density of 280 mAcm^{-2} for methanol oxidation reaction (MOR). Copolymerization of polyaniline and polypyrrole improved the transport of electrical charges and enhanced the specific surface area. This increased surface area allowed for the deposition of nickel nanostructures without agglomeration, improving methanol desorption and adsorption and increased oxidation activity at lower onset potentials and better stability than other electrocatalysts. Thus, the synthesized electrocatalysts have potential applications as an enhanced anode electrode for direct methanol (DMFC) at a reasonable cost because of their electrocatalytic qualities for methanol oxidation reaction.
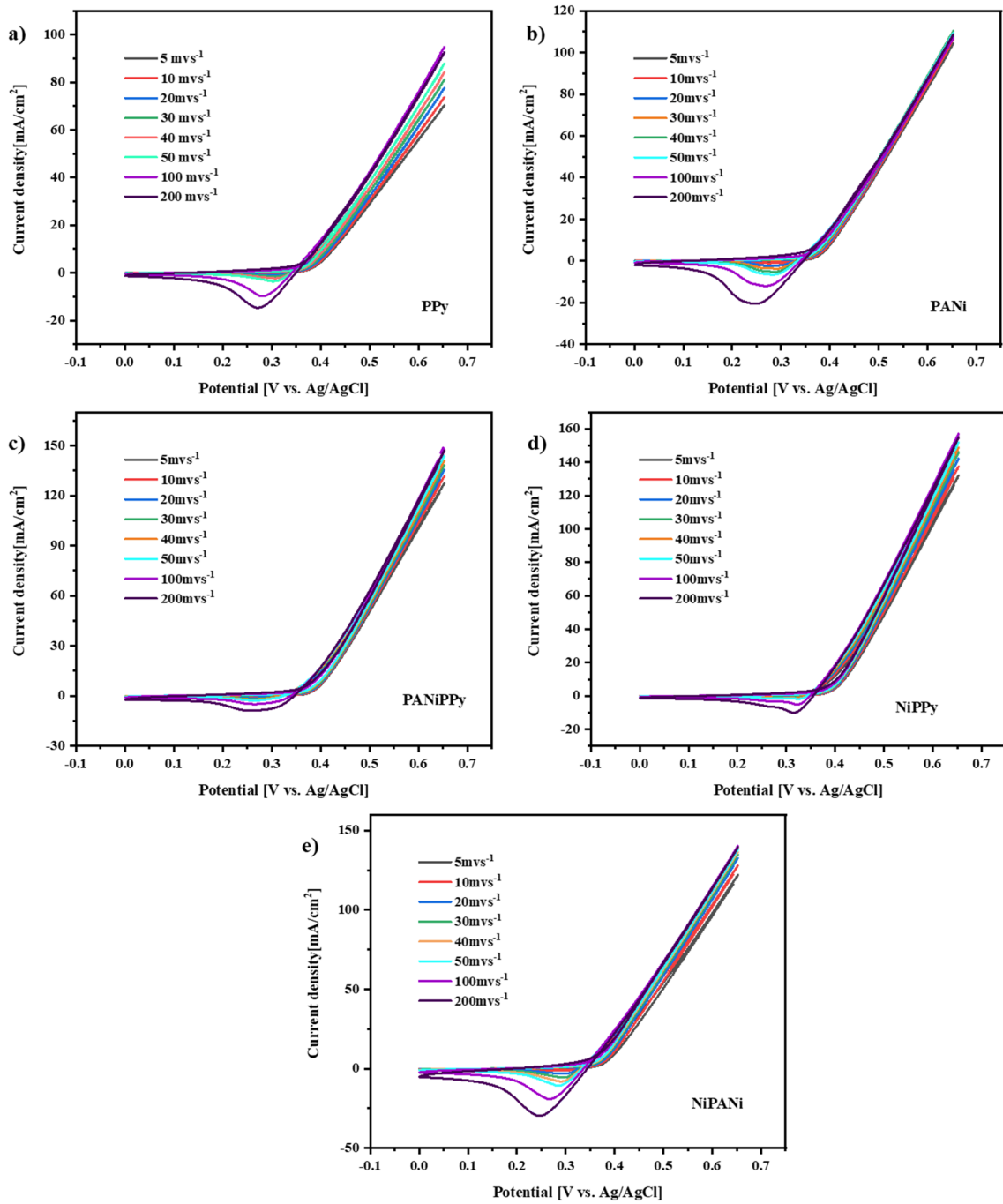
range 0.1 to 10 kHz at 10 mV amplitude. Figure 16 shows Nyquist plots for NiPANiPPy and other electrocatalysts. It has been seen to exhibit a partial semi-circle in the high-frequency area and a linear plot in the low-frequency zone. The electrode material NiPANiPPy has the lowest solution resistance (0.8 Ω cm^{-2}) when compared to other electrocatalysts with solution resistances ranging from 1.5 to 2.5 Ω cm^{-2}. To boost electrooxidation, nickel nanoparticles and conducting polymer work together to increase electron mobility. The inset includes the enlarged Nyquist plot in high-frequency area showcasing the partial semi-circle along with the equivalent circuit of the NiPANiPPy that characterize the resistive or capacitive behavior of the active material and interfaces. In the circuit, Rs is the electrolytic solution resistance (Table 2). Parallel R–C elements are designated as Rp and CPE. Diffusion resistance is assessed by the Warburg element. The R − C elements explain the resistive and

Fig. 13 Cyclic voltammogram of (a) PPy, (b) PANi, (c) PANiPPy, (d) NiPPy, and (e) NiPANi at varying scan rate
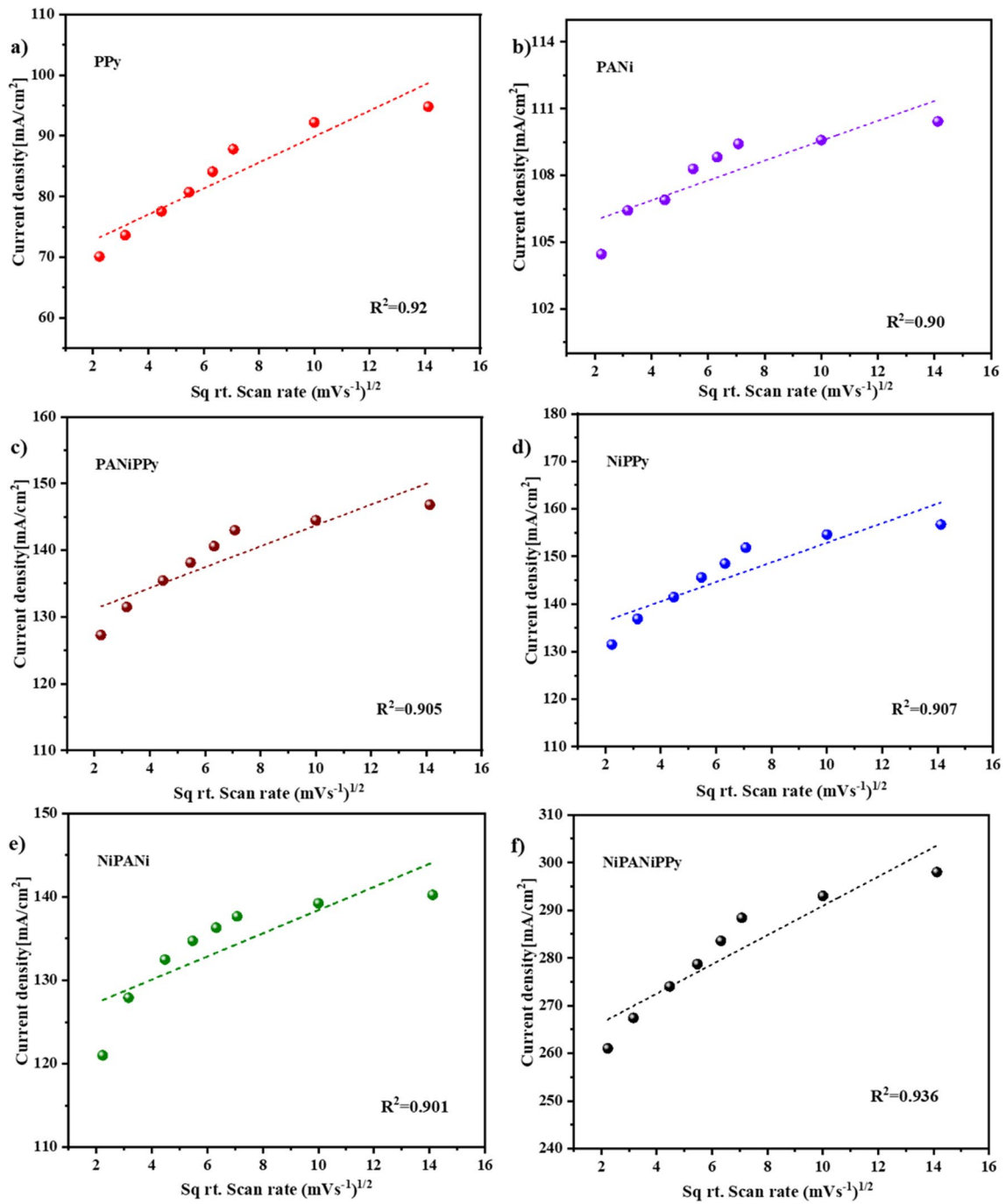
Fig. 14 Plots of current density versus square root of scan rate (a) PPy, (b) PANi, (c) PANiPPy, (d) NiPPy, (e) NiPANi, and (f) NiPANiPPy

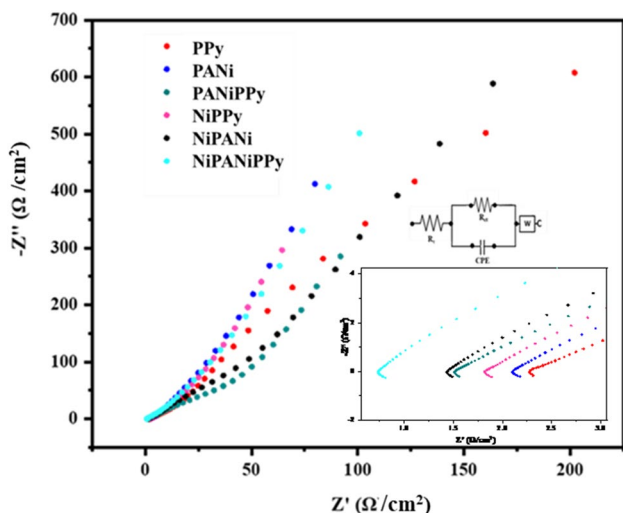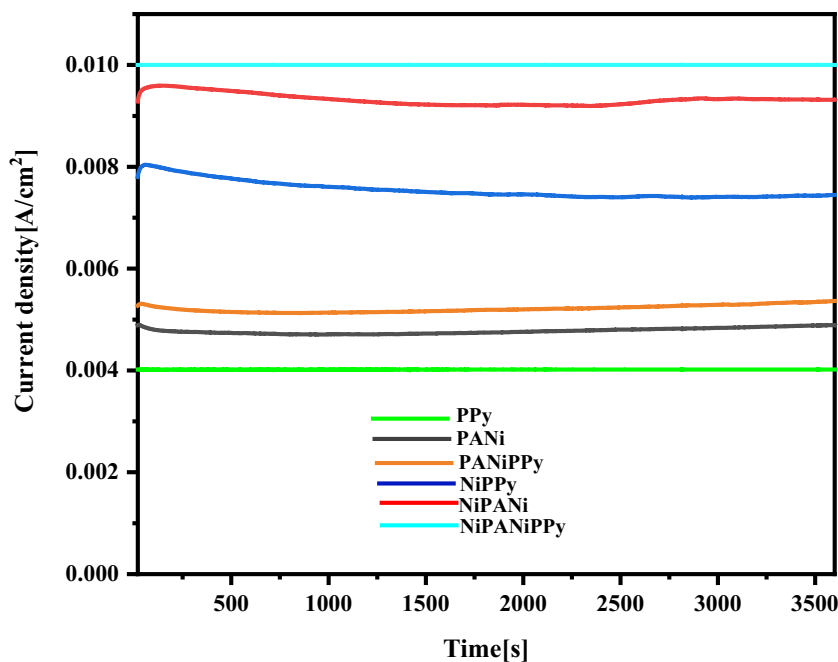**Fig. 15** Chronoamperometric curves of all electrocatalysts

Fig. 16 EIS spectra of PANi, PPy, PANiPPy, NiPANi, NiPPy, and NiPANiPPy

Table 2 Comparison of solution resistance of the synthesised electrocatalysts

Electrocatalysts	Solution resistance (Rs) (ohm cm^{-2})
PPy	2.31
PANi	2.17
PANiPPy	1.558
NiPPy	1.88
NiPANi	1.47
NiPANiPPy	0.8

Declarations

Competing interests The authors declare no competing interests.

Conflict of interest The authors declare no competing interests.

References

1. Jiang R, Chu D (2003) Comparative studies of methanol crossover and cell performance for a DMFC. J Electrochem Soc 151(1):A69
2. Liu H, Song C, Zhang L, Zhang J, Wang H, Wilkinson DP (2006) A review of anode catalysis in the direct methanol fuel cell. J Power Sources 155(2):95–110

3. Natarajan VK, Madaswamy SL, muteb Aljuwayid A, Azam M, Wabaidur SM, Dhanusuraman R (2023) Ultrasound assisted synthesis of cobalt tungstate decorated poly (2, 5-dimethoxyaniline) nanocomposite towards improved methanol electro-oxidation. J Ind Eng Chem 121:480–488

4. Boxall DL, Deluga GA, Kenik EA, King WD, Lukehart C (2001) Rapid synthesis of a Pt1Ru1/carbon nanocomposite using microwave irradiation: A DMFC anode catalyst of high relative performance. Chem Mater 13(3):891–900

5. Raveendran A, Chandran M, Dhanusuraman R (2023) A comprehensive review on the electrochemical parameters and recent material development of electrochemical water splitting electrocatalysts. RSC Adv 13(6):3843–3876

6. Hoel M, Kverndokk S (1996) Depletion of fossil fuels and the impacts of global warming. Resour Energy Econ 18(2):115–136

7. Höök M, Tang X (2013) Depletion of fossil fuels and anthropogenic climate change—A review. Energy Policy 52:797–809

8. Kamarudin SK, Daud WRW, Ho SL, Hasran UA (2007) Overview on the challenges and developments of micro-direct methanol fuel cells (DMFC). J Power Sources 163(2):743–754

9. Chandran M, Raveendran A, Vinoba M, Bhagiyalakshmi M (2023) Design considerations. In: Supercapacitors and their applications. CRC Press, pp 71–86

10. Raveendran A, Chandran M, Siddiqui MR, Wabaidur SM, Eswaran M, Dhanusuraman R (2023) Different electrodeposition techniques of manganese and nickel oxide on nickel foam and their effect on improved supercapacitor behaviour: a comparative study. J Mater Sci Mater Electron 34(30):2018

11. Chandran M, Thomas A, Raveendran A, Vinoba M, Bhagiyalakshmi M (2020) MoS2 confined MXene heterostructures as electrode material for energy storage application. J Energy Storage 30:101446

12. Chandran M, Shamna I, Anusha A, Bhagiyalakshmi M (2019) Synthesis of mesoporous carbon-polymeric hybrid material for energy storage application. SN Appl Sci 1(6):509

13. Nandi D, Mohan VB, Bhowmick AK, Bhattacharyya D (2020) Metal/metal oxide decorated graphene synthesis and application as supercapacitor: a review. J Mater Sci 55(15):6375–6400

14. Raveendran A, Chandran M, Siddiqui MR, Wabaidur SM, Angaiah S, Dhanusuraman R (2024) Binary Ni–cu nanocomposite-modified MXene-adorned 3D-nickel foam for effective overall water splitting and supercapacitor applications. Sustain Energy Fuels 8(7):1509–1525

15. Yan B, Li X, Xiao W, Hu J, Zhang L, Yang X (2020) Design, synthesis, and application of metal sulfides for Li–S batteries: progress and prospects. J Mater Chem A 8(35):17848–17882

16. Larcher D, Beattie S, Morcrette M, Edstroem K, Jumas J-C, Tarascon J-M (2007) Recent findings and prospects in the field of pure metals as negative electrodes for Li-ion batteries. J Mater Chem 17(36):3759–3772

17. Mei J, Liao T, Sun Z (2018) Two-dimensional metal oxide nanosheets for rechargeable batteries. J Energy Chem 27(1):117–127

18. Kamarudin SK, Achmad F, Daud WRW (2009) Overview on the application of direct methanol fuel cell (DMFC) for portable electronic devices. Int J Hydrog Energy 34(16):6902–6916

19. Sivasankarapillai VS, Keertheeswari NV, Chahal P, Wabaidur SM, Ponnusamy VK, Dhanusuraman R (2022) Facile electrodeposition fabrication of raspberry-like gold microspheres decorated polydiphenylamine nanohybrid coated electrode for efficient direct methanol fuel cell application. Fuel 330:125530

20. Raveendran A, Chandran M, Siddiqui MR, Wabaidur SM, Eswaran M, Dhanusuraman R (2023) Layer-by-layer assembly of CTAB-rGO-modified MXene hybrid films as multifunctional electrodes for hydrogen evolution and oxygen evolution reactions, supercapacitors, and DMFC applications. ACS Omega 8(38):34768–34786

21. Madaswamy SL, Vengadesan K, Wabaidur SM, Islam MA, Philips MF, Dhayalan V et al (2022) One-pot electro-codeposition of nanospherical polydiphenylamine-palladium–supported graphitic carbon nitride nanohybrid for efficient methanol oxidation. Ionics 28(10):4697–4708

22. Choi J-H, Kim Y-M, Lee J-S, Cho K-Y, Jung H-Y, Park J-K et al (2005) A polyaniline supported PtRu nanocomposite anode and a Pd-impregnated nanocomposite Nafion membrane for DMFCs. Solid State Ionics 176(39–40):3031–3034

23. Brouzgou A, Song S, Tsiakaras P (2012) Low and non-platinum electrocatalysts for PEMFCs: current status, challenges and prospects. Appl Catal B Environ 127:371–388

24. Raveendran A, Chandran M, Wabaidur SM, Islam MA, Dhanusuraman R, Ponnusamy VK (2022) Facile electrochemical fabrication of nickel-coated Polydiphenylamine (Ni/PDPA) nanocomposite material as efficient anode catalyst for direct alcohol fuel cell application. Fuel 324:124424

25. Natarajan VK, Madaswamy SL, Krishnamoorthy N, Ramamoorthy G, Dhanusuraman R (2023) Ultrasonicationassisted synthesis of nickel tungstate decorated on polydimethoxyaniline nanocomposite catalyst for potential direct methanol fuel cell application. ES Energy Environ 21(3):926

26. Xu C, Hu Y, Rong J, Liu Y (2007) Ni hollow spheres as catalysts for methanol and ethanol electrooxidation. Electrochem Commun 9(8):2009–2012

27. Chandran M, Raveendran A, Vinoba M, Vijayan BK, Bhagiyalakshmi M (2021) Nickel-decorated MoS2/MXene nanosheets composites for electrocatalytic oxidation of methanol. Ceram Int 47(19):26847–26855

28. Dhanusuraman R, Chahal P, Raveendran A, Hossain M, Alshgari RA, Wabaidur SM et al (2023) Facile fabrication of platinum loaded poly (2, 5-dimethoxy aniline)/activated carbon ternary nanocomposite as an efficient electrode material for high performance supercapacitors. J Energy Storage 60:106554

29. Ragupathy D, Gopalan AI, Lee K-P, Manesh KM (2008) Electro-assisted fabrication of layer-by-layer assembled poly (2, 5-dimethoxyaniline)/phosphotungstic acid modified electrode and electrocatalytic oxidation of ascorbic acid. Electrochem Commun 10(4):527–530

30. Raveendran A, Chandran M, Lee SC, Siddiqui MR, Wabaidur SM, Dhanusuraman R (2024) Self-supported 3D corallike copper/poly diphenylamine on nickel foam: multifunctional exploration of overall electrochemical water splitting, alcohol oxidation reaction and supercapacitor applications. New J Chem 48(5):2236–2250

31. Ragupathy D, Gomathi P, Lee SC, Al-Deyab SS, Lee SH, Do GH (2012) One-step synthesis of electrically conductive polyaniline nanostructures by oxidative polymerization method. J Ind Eng Chem 18(4):1213–1215

32. Sadki S, Schottland P, Brodie N, Sabouraud G (2000) The mechanisms of pyrrole electropolymerization. Chem Soc Rev 29(5):283–293

33. Choi YS, Joo SH, Lee S-A, You DJ, Kim H, Pak C et al (2006) Surface selective polymerization of polypyrrole on ordered mesoporous carbon: enhancing interfacial conductivity for direct methanol fuel cell application. Macromolecules 39(9):3275–3282

34. Ben Jadi S, El Guerraf A, Bazzaoui E, Wang R, Martins J, Bazzaoui M (2019) Synthesis, characterization, and transport properties of Nafion-polypyrrole membrane for direct methanol fuel cell (DMFC) application. J Solid State Electrochem 23:2423–2433

35. Vengadesan K, Madaswamy SL, Lee SC, Siddiqui MR, Dhanusuraman R, Ponnusamy VK (2023) One-step fabrication of poly (aniline-co-2, 5 dimethoxyaniline) nanohybrid coated graphitic sheet electrode for efficient energy application. Int J Hydrog Energy 48(55):21018–21028

36. Quillard S, Louarn G, Lefrant S, MacDiarmid A (1994) Vibrational analysis of polyaniline: A comparative study of leucoemeraldine, emeraldine, and pernigraniline bases. Phys Rev B 50(17):12496

37. Das S, Dutta K, Kundu PP (2016) Sulfonated polypyrrole matrix induced enhanced efficiency of Ni nanocatalyst for application as an anode material for DMFCs. Mater Chem Phys 176:143–151.

38. Pattanayak P, Pramanik N, Kumar P, Kundu PP (2018) Fabrication of cost-effective non-noble metal supported on conducting polymer composite such as copper/polypyrrole graphene oxide (Cu2O/PPy–GO) as an anode catalyst for methanol oxidation in DMFC. Int J Hydrog Energy 43(25):11505–11519.

39. Kuila T, Sheng YD, Murmu NC (2015) Graphene/conjugated polymer nanocomposites for optoelectronic and biological applications. Copolymers and Composites, Fundamentals of Conjugated Polymer Blends, pp 229–279

40. Tang Q, Wu J, Li Y, Lin J, Tang Z, Huang M (2011) Facile secondary-template synthesis of polyaniline microtube array for enhancing glucose biosensitivity. J Mater Chem 21(34):12927–12934

41. Solanki PR, Singh S, Prabhakar N, Pandey M, Malhotra B (2007) Application of conducting poly (aniline-co-pyrrole) film to cholesterol biosensor. J Appl Polym Sci 105(6):3211–3219

42. Sudhasree S, Shakila Banu A, Brindha P, Kurian GA (2014) Synthesis of nickel nanoparticles by chemical and green route and their comparison in respect to biological effect and toxicity. Toxicol Environ Chem 96(5):743–754

43. Şen S, Gök A, Gülce H (2007) Novel Ni/polypyrrole and cu/polypyrrole composites prepared in the presence of different acids: synthesis and investigation of thermal stability. J Appl Polym Sci 106(6):3852–3860

44. Abdolahi A, Hamzah E, Ibrahim Z, Hashim S (2012) Synthesis of uniform polyaniline nanofibers through interfacial polymerization. Materials 5(8):1487–1494

45. Ramesan MT (2012) In situ synthesis, characterization and conductivity of copper sulphide/polypyrrole/polyvinyl alcohol blend nanocomposite. Polym-Plast Technol Eng 51(12):1223–1229

46. Mažeikienė R, Niaura G, Malinauskas A (2021) Poly (N-methyl-aniline) vs. polyaniline: an extended pH range of polaron stability as revealed by Raman spectroelectrochemistry. Spectrochim Acta A Mol Biomol Spectrosc 262:120140

47. Pattanayak P, Papiya F, Kumar V, Singh A, Kundu PP (2021) Performance evaluation of poly (aniline-co-pyrrole) wrapped titanium dioxide nanocomposite as an air-cathode catalyst material for microbial fuel cell. Mater Sci Eng C 118:111492.

48. Mikat J, Orzgall I, Hochheimer H (2002) Raman spectroscopy of conducting polypyrrole under high pressure. Phys Rev B 65(17):174202

49. Abdullah HS (2012) Electrochemical polymerization and Raman study of polypyrrole and polyaniline thin films. Int J Phys Sci 7(38):5468–5476

50. Chaudhary S, Kiran Kumar A, Sharma ND, Gupta M (2019) Cauliflower-shaped ternary nanocomposites with enhanced power and energy density for supercapacitors. Int J Energy Res 43(8):3446–3460

51. Vinodh R, Babu RS, Atchudan R, Kim H-J, Yi M, Samyn LM et al (2022) Fabrication of high-performance asymmetric supercapacitor consists of nickel oxide and activated carbon (NiO//AC). Catalysts 12(4):375

52. Vinodh R, Rana PJS, Muralee Gopi CV, Yang Z, Atchudan R, Venkatachalam K et al (2019) Polyaniline–13X zeolite composite-supported platinum electrocatalysts for direct methanol fuel cell applications. Polym Int 68(5):929–935

53. Fleischmann M, Korinek K, Pletcher D (1971) The oxidation of organic compounds at a nickel anode in alkaline solution. J Electroanal Chem Interfacial Electrochem 31(1):39–49

54. Sheikhi S, Jalali F (2021) Zr-MOF@ polyaniline as an efficient platform for nickel deposition: application to methanol electro-oxidation. Fuel 296:120677

55. Fard LA, Ojani R, Raoof JB, Zare EN, Lakouraj MM (2017) Poly (pyrrole-co-aniline) hollow nanosphere supported Pd nanoflowers as high-performance catalyst for methanol electrooxidation in alkaline media. Energy 127:419–427

56. Magal RT, Selvaraj V (2018) A comparative study for the electrocatalytic oxidation of alcohol on Pt-Au nanoparticlesupported copolymer-grafted graphene oxide composite for fuel cell application. Ionics 24(5):1439–1450

57. Wu T-Y, Chen B-K, Chang J-K, Chen P-R, Kuo C-W (2015) Nanostructured poly (aniline-co-metanilic acid) as platinum catalyst support for electro-oxidation of methanol. Int J Hydrog Energy 40(6):2631–2640

58. Pandey RK, Lakshminarayanan V (2012) Ethanol electrocatalysis on gold and conducting polymer nanocomposites: A study of the kinetic parameters. Appl Catal B Environ 125:271–281

59. Chemchoub S, Oularbi L, El Attar A, Younssi SA, Bentiss F, Jama C et al (2020) Cost-effective non-noble metal supported on conducting polymer composite such as nickel nanoparticles/polypyrrole as efficient anode electrocatalyst for ethanol oxidation. Mater Chem Phys 250:123009

60. Soleimani-Lashkenari M, Rezaei S, Fallah J, Rostami H (2018) Electrocatalytic performance of Pd/PANI/TiO2 nanocomposites for methanol electrooxidation in alkaline media. Synth Met 235:71–79

61. Ghosh S, Das S, Mosquera ME (2020) Conducting polymer-based nanohybrids for fuel cell application. Polymers 12(12):2993